J. Fluid Mech. (1995), *vol.* 283, *pp.* 97–123

Nonlinear instability of liquid jets with thermocapillarity

By F. MASHAYEK AND N. ASHGRIZ

Department of Mechanical and Aerospace Engineering, State University of New York at Buffalo, Buffalo, NY 14260, USA

(Received 1 March 1994 and in revised form 29 July 1994)

The breakup mechanism of a capillary jet with thermocapillarity is investigated. Effects of the heat transfer from the liquid to the surrounding ambient, the liquid thermal conductivity, and the temperature-dependent surface tension coefficient on the jet instability and the formation of satellite drops are considered. Two different disturbances are imposed on the jet. In the first case, the jet is exposed to a spatially periodic ambient temperature. In addition to the thermal boundary condition, an initial surface disturbance with the same wavenumber as the thermal disturbance is also imposed on the jet. Both in-phase and out-of-phase thermal disturbances with respect to surface disturbances are considered. For the in-phase thermal disturbances, a parameter set is obtained at which capillary and thermocapillary effects can cancel each other and the jet attains a stable configuration. No such parameter set can be obtained when the thermocapillary flows are in the same direction as the capillary flows, as in the out-of-phase thermal disturbances. In the second case, only an initial thermal disturbance is imposed on the surface of the liquid while the ambient temperature is kept spatially and temporally uniform.

1. Introduction

More than a century after Rayleigh's (1879) first paper on the instability of an isothermal liquid jet, Bauer (1984), Xu & Davis (1985), and, more recently, Dijkstra & Steen (1991) considered the 'linear' instability of a non-isothermal jet with temperature-dependent surface tension coefficient. Here, we present a nonlinear analysis for instability of such jets.

In non-isothermal capillary jets, variation of the surface tension with temperature along the free surface of the liquid results in a tangential shear force on the surface which induces the so-called thermocapillary flows (Ostrach 1982; Davis 1987). Thermocapillary effects can, depending on the particular conditions, enhance or retard the instability. The former effect can be used in controlling the breakup of the liquid jets, and the latter to attain long and stable liquid columns. The controlled breakup of the liquid jets is mainly utilized in the production of spherical drops, such as in ink jet printers and in the manufacturing of microspheres. On the other hand, more stable and long liquid columns are useful in such processes as containerless processing of single crystals, wave soldering, and liquid metal spinning. These processes are dependent on the length and stability of the liquid column that can be sustained in an ambient with varying temperature.

Techniques used to control the breakup of a liquid jet are mainly based on applying a periodic disturbance on the jet surface or the liquid supply system. Surface, pressure, or velocity disturbances have been commonly utilized. It is conceivable, however, to

develop a technique based on disturbing the liquid properties, such as the liquid surface tension. Since, the liquid surface tension is strongly dependent on the temperature, it can be controlled by controlling the liquid temperature. This technique was utilized by Faidley & Panton (1990) to control the breakup of a water jet. They used a small, fast-responding heater at the orifice of a nozzle to modulate the surface tension along a jet of water issuing into air. Their results indicated that the Rayleigh instability mode was dominant in this case and no significant variation in the growth rates was observed. This was attributed to the lack of sufficient power in the heating element to excite another instability mode. Later Nahas & Panton (1991) used laser radiation in order to better control the changes in the liquid surface tension. A CO_2 laser beam modulated at the same frequency as the primary surface disturbance was focused on the surface of the jet. They were able to cancel the primary surface disturbance by an appropriate adjustment of the laser intensity and phase. This technique shows promise as an alternative method for controlling the breakup of a liquid jet.

The instability studies of isothermal liquid jets using an initial disturbance with known amplitude and wavelength are exemplified by the analytical investigation of Rayleigh (1879), Yuen (1968), and Chaudhary & Redekopp (1980); experimental studies of Plateau (1873), Goedde & Yuen (1970), and Vassallo & Ashgriz (1991); and numerical simulations of Fromm (1984), Shokoohi & Elrod (1987), Mansour & Lundgren (1990), and Ashgriz & Mashayek (1994). All these studies have considered a jet with constant liquid properties.

Compared to the isothermal jet instability, there is very limited number of studies on the non-isothermal jets. Bauer (1984) provided the first study on the linear instability of an infinitely long axisymmetric liquid jet or column with a temperature-dependent surface tension coefficient. He assumed a creeping flow and imposed an arbitrary axially periodic temperature field on the liquid surface, and obtained an analytical solution for the growth rate of the disturbances. He concluded that the breakup of a liquid jet may occur not only for surface amplitude disturbances with axial wavelengths larger than the circumference of the jet, but also through oscillatory temperature gradients that excite the otherwise calm free surface. Later, Xu & Davis (1985, hereinafter referred to as XD) considered a linear temperature gradient along the liquid surface. Using a lubrication theory, they found the velocity and temperature distributions inside the jet due to a convective heat transfer with the ambient. This was used as the basic state for the jet. They found that the capillary instabilities can be greatly retarded or even suppressed by surface wave instabilities. Similar stabilizing effects have been observed by Russo & Steen (1989) in the study of the capillary breakup of long liquid cylinders subject to a shear on the surface. They showed that for a certain range of non-dimensional parameters the addition of surface waves, produced by the applied shear on the surface of the cylinder, stabilized the capillary waves. Later, Dijkstra & Steen (1991) considered the thermocapillary stabilization of annular films of liquids. Similarly to XD, base flows were generated by a gradient in surface tension induced by a linear temperature gradient along the interface. Using a linear stability analysis, they showed that complete stabilization is achieved due to the thermocapillary-driven motions.

In addition to the above-mentioned studies, many other investigators have reported on general thermocapillary flows. These have been mainly in two- or three-dimensional planar liquid layers or in short and stable cylindrical liquid columns. For instance, Sen & Davis (1982) studied the flow of a liquid in a two-dimensional slot subject to a temperature gradient on the surface. They assumed small aspect ratios, A = depth/length, and developed an asymptotic theory which was valid for $A \to 0$. The

capillary number was also assumed to be very small which implied very large mean surface tension and, therefore, very small surface deformations were allowed. Cowley & Davis (1983) considered the liquid lying in a quarter-plane with a non-deflecting thermally insulated interface. The sidewall was insulated and held at a fixed temperature. They found that the strongest thermocapillary flows were confined to very small corner region which resulted in the worst convection-generated defect in crystal growth.

The instability of both two- and three-dimensional sheared liquid layers subject to a temperature gradient along the layer were studied in detail by Smith & Davis (1982, 1983*a*, *b*). For three-dimensional layers, they identified two broad classes of instabilities. The first was a convective or thermal instability whose mechanism involved a balance between heat conduction and heat convection at the free surface and was relatively unaffected by the free surface deformation. The second class was a surface wave instability whose mechanism involved the mechanical transfer of momentum from the basic state to the disturbances and was highly dependent on the free surface deformations. The thermal instabilities were of two types: (i) stationary longitudinal rolls produced in a layer heated from below, and (ii) propagating hydrothermal waves which derived their energy from the imposed horizontal temperature gradient when the Prandtl number of the liquid was small and from a vertical temperature gradient when the Prandtl number was large. Later, Smith (1986) described the physical mechanism for the hydrothermal wave instability in dynamic thermocapillary liquid layers by considering low and large Prandtl number liquids.

The study of thermocapillary-induced flows was then extended to axisymmetric liquid bridges by Xu & Davis (1983) who assumed an axial temperature gradient. They relaxed the limiting assumptions for capillary, Reynolds, and Marangoni numbers, and allowed large surface deformations, but considered the core flows only away from the endwalls. Xu & Davis (1984), using the same basic state as stated earlier for XD, studied the convective thermocapillary instability in liquid bridges. They ignored the presence of the endwalls of the zone, the interfacial deformation, and gravity. They obtained axisymmetric waves which propagated against the surface flow for large Prandtl numbers.

Numerical investigations of thermocapillary-induced flows are also largely devoted to liquid columns. Cuvelier & Driessen (1986) studied the two-dimensional steady thermocapillary flow in a column for a large group of non-dimensional parameters. They used the finite element method along with three different iterative methods for the computation of the free boundary. They concluded that for melts with low Prandtl numbers the temperature distribution is almost independent of the flow, because heat is mainly transferred by conduction. However, for high Prandtl number liquids, convective heat transfer is significant and the isotherms become more distorted. Energy stability theory was used by Shen *et al.* (1990) to investigate the stability of a cylindrical half-zone of finite length subject to thermocapillary convection. They obtained values of the Marangoni number below which axisymmetric disturbances decayed, for various values of other significant parameters.

Kazarinoff & Wilkowski (1990) studied the bifurcation of thermocapillary flows in axisymmetric float zones and indicated that the aspect ratio (ratio of the length to radius) plays a critical role. Their numerical technique was a hybrid of finite difference and finite element methods – the latter was used to determine the location of the free surface. Thermocapillary convection in layers with small depth and subject to a horizontal temperature gradient was studied by Hadid & Roux (1990) using a finite difference technique. They observed multi-roll structure near the cold endwall, with the

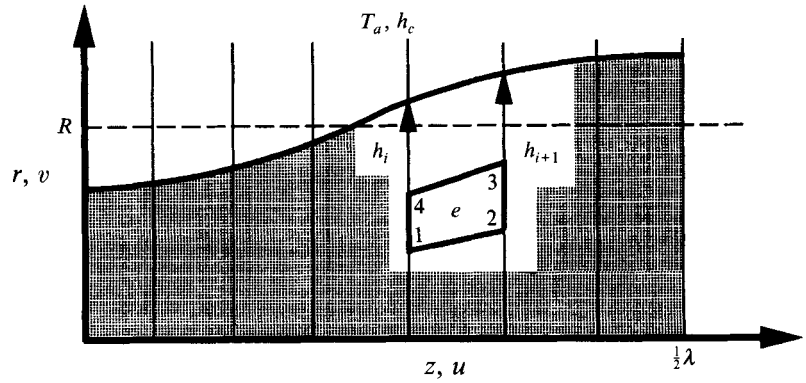

FIGURE 1. The fluid zone is confined to the free surface, at the top, which is represented by heights h. A typical bilinear element e used for simulations is also shown on the figure with its corresponding local node numbering. λ is the disturbance wavelength and R is the initial non-disturbed radius of the jet. A convective heat transfer with the ambient at temperature T_a is considered with the coefficient of convective heat transfer h_c.

number of rolls increasing with Reynolds number. Doi & Koster (1993) considered thermocapillary-induced flows in two immiscible liquid layers with one free surface and one liquid/liquid interface. A 'halt' condition was found that prevented the motion of the liquid in the lower encapsulated liquid layer. Kuhlmann & Rath (1993) solved for the basic state and the three-dimensional disturbance equations by various spectral methods to study the hydrodynamic instabilities in cylindrical thermocapillary bridges. They found that critical modes have azimuthal wavenumber of one and the most dangerous disturbance was either a pure hydrodynamic steady mode or an oscillatory hydrothermal wave, depending on the Prandtl number.

In this paper the temporal instability of a liquid jet, or a long liquid column, with thermocapillarity subject to periodic disturbances is investigated. The objectives are to identify the effects of various parameters on the nonlinear thermocapillary instability of liquid jets and the formation of the satellite drops; and to identify the thermal disturbances which either favour the breakup of liquid jets or help the formation of more stable liquid columns. Both thermal and surface disturbances are used. In §2 the mathematical formulation of the problem is provided along with a description of the numerical procedure. In §3 the jet is exposed to an ambient with spatially periodic temperaure distribution, while in §4 the instability of the jet in a spatially and temporally uniform ambient and subject to an initial thermal (as well as surface) disturbance is investigated. Discussion and conclusions are given in §5.

2. Mathematical and numerical formulation

The temporal instability of a thermocapillary jet in a dynamically inactive ambient and in the absence of gravity is investigated. We consider an axisymmetric laminar flow of a viscous incompressible liquid jet which is stationary relative to a moving observer. The liquid is Newtonian with constant viscosity μ, density ρ, specific heat c_p, and thermal conductivity κ. The liquid surface tension, α', is assumed to be a linear function of temperature: $\alpha' = \alpha'_0 - \gamma(T' - T'_0)$, where T' is the liquid temperature, α'_0 is the surface tension coefficient at a reference temperature T'_0 (in §3, T'_0 is defined as the lowest temperature in the ambient, and in §4, as the initial temperature of the liquid),

and γ is the rate of change of surface tension coefficient with temperature. The length, time, velocity, and pressure are scaled by R_0', $\mu R_0'/\gamma\Delta T'$, $\gamma\Delta T'/\mu$, and $\gamma\Delta T'/R_0'$, respectively, where R_0' is the unperturbed radius of the axisymmetric liquid jet, and $\Delta T'$ is a characteristic temperature difference. In §3 $\Delta T'$ is defined as the difference between the initial temperature of the jet and T_0', and in §4 it is defined as the difference between the ambient temperature and T_0'. In addition, temperature is non-dimensionalized as $T = (T' - T_0')/\Delta T'$. Consequently, the following dimensionless numbers are obtained:

$$Re = \frac{\rho\gamma\Delta T' R_0'}{\mu^2}, \quad Ca = \frac{\gamma\Delta T'}{\alpha_0'}, \quad Ma = Re\,Pr, \quad Bi = \frac{h_c R_0'}{\kappa}, \tag{1}$$

where Re, Ca, Ma, $Pr = \mu c_p/\kappa$, and Bi are the Reynolds, capillary, Marangoni, Prandtl, and Biot numbers, respectively. Here, a convective heat transfer with the surrounding gas at temperature T_a', and with constant convective heat transfer coefficient h_c is assumed. T_a' is not constant in general and may vary with the axial coordinate z. The variation of the surface tension with temperature in non-dimensional form is

$$\alpha = \alpha'/\alpha_0' = 1 - Ca\,T. \tag{2}$$

The governing equations for the flow are the continuity, momentum, and energy equations which are stated in dimensionless form as follows:

$$\nabla\cdot\boldsymbol{u} = 0, \tag{3}$$

$$Re\,\mathrm{D}\boldsymbol{u}/\mathrm{D}t = \nabla\cdot\boldsymbol{\sigma}, \tag{4}$$

$$Ma\,\mathrm{D}T/\mathrm{D}t = \nabla^2 T, \tag{5}$$

where $\boldsymbol{u} = (u, v)$ is the velocity vector in axisymmetric coordinate (z, r),

$$\boldsymbol{\sigma} = -p\boldsymbol{I} + [\nabla\boldsymbol{u} + (\nabla\boldsymbol{u})^T]$$

is the stress tensor for Newtonian fluid, and $\mathrm{D}/\mathrm{D}t = \partial/\partial t + \boldsymbol{u}\cdot\nabla$ is the total derivative operator with ∇ being the gradient operator.

The stress balance on the free surface provides the following boundary conditions (assuming the ambient pressure as the datum):

$$\boldsymbol{\sigma}\cdot\boldsymbol{n} = F_n\boldsymbol{n} + F_t\boldsymbol{t}, \tag{6a}$$

where

$$F_n = \frac{1 - CaT}{Ca\,Re}K, \quad F_t = \frac{1}{Re}\frac{T_z + h_z T_r}{(1 + h_z^2)^{1/2}}; \tag{6b, c}$$

$\boldsymbol{n}$ and $\boldsymbol{t}$ are the outward unit normal and tangent to the surface, respectively, and K is the curvature of the surface. Subscripts z and r refer to partial derivatives in the z- and r-directions, respectively. The free surface is represented by a height function $h(z, t)$ (Mashayek & Ashgriz 1993), which is independent of the radius r, as shown in figure 1. Therefore, K is given by

$$K = \frac{h_{zz}}{(1 + h_z^2)^{3/2}} - \frac{1}{h(1 + h_z^2)^{1/2}}. \tag{7}$$

The convective heat transfer with the ambient is described by

$$\nabla T\cdot\boldsymbol{n} = \frac{Bi}{Ma}(T_s - T_a), \tag{8}$$

where T_s is the temperature of the liquid at the free surface. Since a temporal analysis

is considered here, the symmetry boundary conditions are applied both on the axis of the symmetry z, and on the end planes of the half-wavelength:

$$\frac{\partial u}{\partial r} = 0, \quad v = 0, \quad \frac{\partial T}{\partial r} = 0 \quad \text{at} \quad r = 0, \tag{9}$$

$$u = 0, \quad \frac{\partial v}{\partial z} = 0, \quad \frac{\partial T}{\partial z} = 0 \quad \text{at} \quad z = 0, \lambda/2, \tag{10}$$

where λ is the non-dimensional disturbance wavelength.

A Galerkin finite element method is used to solve (3)–(5). Four-node bilinear isoparametric elements are used to approximate the velocity and temperature distribution over each element:

$$\boldsymbol{u}(z, r, t) = \sum_{i=1}^{4} \boldsymbol{u}_i(t)\, N_i(z, r, t), \tag{11}$$

$$T(z, r, t) = \sum_{i=1}^{4} T_i(t)\, N_i(z, r, t). \tag{12}$$

A moving mesh is used to discretize the computational domain, resulting in time-dependent shape functions. For the momentum equation a penalty function formulation is implemented where the pressure is eliminated from the set of unknown variables by absorbing the continuity equation (3) into the momentum equation (4). Therefore, the pressure is defined as

$$p = -\Upsilon \nabla \cdot \boldsymbol{u}, \tag{13}$$

where Υ is a large number ($\sim O(10^{10})$) depending on μ and Re (Hughes, Liu & Brooks 1979). The following closed-form finite element formulations for the velocity and temperature fields are derived:

$$\int_{\Omega(t)} \left(N_j Re \frac{\mathrm{D}\boldsymbol{u}}{\mathrm{D}t} + \nabla N_j^T \cdot [\Upsilon(\nabla \cdot \boldsymbol{u})\boldsymbol{I} + [\nabla \boldsymbol{u} + (\nabla \boldsymbol{u})^T]] \right) \mathrm{d}\Omega = \int_{\Gamma(t)} N_j (F_n \boldsymbol{n} + F_t \boldsymbol{t})\, \mathrm{d}\Gamma, \tag{14}$$

$$\int_{\Omega(t)} \left(N_j Ma \frac{\mathrm{D}T}{\mathrm{D}t} + \nabla N_j \cdot \nabla T \right) \mathrm{d}\Omega = \int_{\Gamma(t)} N_j \frac{Bi}{Ma} (T_s - T_a)\, \mathrm{d}\Gamma, \tag{15}$$

where Ω and Γ are the element volume and boundary, respectively. The above formulation is based on the Eulerian or fixed mesh where the locations of the nodes do not change with time. Special treatment of time derivatives is necessary when a moving grid is considered. Since the shape function has time dependency the time derivative of velocity in discretized form becomes

$$\frac{\partial \boldsymbol{u}}{\partial t} = \sum_{i=1}^{4} \frac{\mathrm{d}\boldsymbol{u}_i}{\mathrm{d}t} N_i + \sum_{i=1}^{4} \boldsymbol{u}_i \frac{\partial N_i}{\partial t}. \tag{16}$$

The last term of (16) introduces a new convective term in (14). Here, motion of the nodes in the r-direction only is allowed according to the following simple rule:

$$z_i(t + \delta t) = z_i(t) = \text{constant}, \quad r_i(t + \delta t) = c r_i(t), \tag{17}$$

where the subscript i refers to the node number, and $c = (z, t)$ is a constant for each column of nodes in the radial direction defined as

$$c = \frac{h(z, t + \delta t)}{h(z, t)}. \tag{18}$$

Mesh	Breakup time	Surface radius at $z = \frac{1}{2}\lambda$	Surface temperature at $z = 0$
40×4	24.229	0.351 22	0.064 51
40×6	24.241	0.350 00	0.062 58
40×7	24.242	0.349 66	0.062 28

TABLE 1. The effect of mesh refinement on the accuracy of the results

Mashayek & Ashgriz (1993) have shown that the total derivative of velocity in this case becomes

$$\frac{\mathrm{D}\boldsymbol{u}}{\mathrm{D}t} = \frac{\partial \boldsymbol{u}}{\partial t} + u\frac{\partial \boldsymbol{u}}{\partial z} + \left(v - \frac{c-1}{\delta t}r\right)\frac{\partial \boldsymbol{u}}{\partial r}. \tag{19}$$

Convective terms in the energy equation are modified similarly.

A detailed code validation is provided in Mashayek (1994) and is not repeated here. It suffices to mention that the results of our code for the thermocapillary flows in finite-length liquid columns are compared with those of Xu & Davis (1983), Fu & Ostrach (1985), Kuhlmann (1989), Shen *et al.* (1990), and Kuhlmann & Rath (1993). The convective heat transfer from the ambient to a liquid column with its ends held at constant temperatures of $T(z = 0) = -0.5$ and $T(z = 1) = 0.5$ is analysed. The surface of the column is assumed to be non-deformable and a linear variation for the ambient temperature is assumed as $T_a(z) = z - 0.5$. The agreement between our solution and theirs is very good; however, we find a better agreement with the spectral solution of Kuhlmann & Rath (1993) than the finite difference calculations of Shen *et al.* (1990). For instance, the measured temperature from the isotherm plot given by Kuhlmann & Rath at $z = 0.536$ and $r = 1$ (on the surface) is 0.1 which is in very good agreement with 0.0991 obtained in our simulation. Also, at $z = 0.832$ and $r = 0$ (on the axis of symmetry), $T = 0.4$ from their results which compares very well with $T = 0.4007$ obtained here.

The test simulations were performed on a 22×20 finite element mesh with compressed elements close to the endwalls and the free surface to resolve the hydrodynamic and thermal boundary layers formed in these regions. For the simulations considered here, the aspect ratio (or the wavelength/radius in the context of the infinite jet) is larger than unity and the flow is more aligned with the axial direction. Typically, 7 to 10 elements in the radial direction were found to be appropriate for aspect ratios about 4 (wavenumbers about 0.8) along with 40 elements in the axial direction. However, the appropriate mesh depends on the initial and boundary conditions and for each particular case is found by comparing the results of simulations performed on meshes with different resolutions. Typical results for a jet with $Re = 20$, $Ma = 200$, $Ca = 0.2$, $Bi = 10$ and $k = 0.7$ are given in table 1 (a detailed description of the problem is given in §3.1). Table 1 indicates good accuracy with 40×7 element mesh and so this has been used for the simulations described in §3.1.

3. Spatially periodic ambient temperature

Consider a jet with an initial surface disturbance of

$$r(z) = R - \epsilon_0 \cos(kz), \tag{20}$$

where ϵ_0 is the initial amplitude of the disturbance and R is determined such that the volume is conserved when the initial amplitude is varied, i.e. $R = (1 - \frac{1}{2}\epsilon_0^2)^{1/2}$. In the

temporal study of a liquid jet, owing to the symmetry only half of one wavelength is sufficient in the analysis. The trough of the initial surface is set at $z = 0$ where $T_a(0) = 0$, and the crest is at $z = \frac{1}{2}\lambda$ where $T_a(\frac{1}{2}\lambda) = 1$ (figure 1). Hereinafter, the initial crest of the sinusoidal surface is referred to as the swell and its trough is referred to as the neck.

In this section we study the instability of the jet when exposed to an ambient with spatially periodic temperature $T_a(z)$ given by

$$T_a(z) = 0.5[1 - \cos(kz + \theta)], \tag{21}$$

where θ is the phase difference between the period of the ambient temperature variation and the period of the surface disturbance (20). In order to retain the symmetric boundary conditions in our temporal analysis, we can only investigate $\theta = 0$ and $\theta = 180°$.

3.1. *In-phase thermal and surface disturbances* ($\theta = 0$)

The problem is characterized by non-dimensional numbers *Re*, *Ma*, *Ca*, *Bi*, and the wavenumber $k = 2\pi/\lambda$. We assume that the jet initially is at a higher temperature than the ambient with $T(r, z) = 1$. The reference temperature, T'_0, is defined as the lowest temperature in the ambient, i.e. $T'_0 = T'_a(z = 0)$, and the characteristic temperature difference, $\Delta T'$, is defined as the difference between the initial temperature of the jet and the reference temperature, i.e. $\Delta T' = T'(t = 0) - T'_0$.

3.1.1. *Marginally stable jets*

From the set of parameters affecting the behaviour of a liquid jet we confine our study to *Bi*, *Ma*, and *Ca*. The other parameters are fixed at $Re = 20$ and $k = 0.7$. Other studies on the capillary jet instability (e.g. Chandrasekhar 1961; Ashgriz & Mashayek 1994) have revealed that the dynamics of a liquid jet does not change significantly for $Re > 10$. At lower *Re*, disturbances grow at much smaller rates. In addition, the maximum growth rate for the capillary jets with $Re \sim O(10)$ occurs around $k = 0.7$. Hence, $Re = 20$ and $k = 0.7$ are chosen for the base case – the wavenumber effect is investigated in §3.1.2.

For $\theta = 0$ the neck is exposed to a lower surrounding temperature than the swell. Therefore, the thermal disturbance presented by (21) induces a thermocapillary flow (from higher surface temperature at the swell towards the lower surface temperature at the neck) in the opposite direction to the capillary flow (from smaller radius at the neck towards the larger radius at the swell). The relative magnitude of these two flows determines the behaviour of the jet. We call the fluid motion induced by the surface displacement 'capillary flows' and that induced by the temperature dependency of the surface tension coefficient 'thermocapillary flows'. The two flows are directly coupled and the distinction is made only for descriptive purposes. Figure 2 shows the time sequence of the evolution of the jets with $Re = 20$, $Ma = 200$, $Ca = 0.2$, $k = 0.7$, $\epsilon_0 = 0.05$, and for various *Bi*. For the jet shown in figure 2(*a*) no heat transfer with the outside is allowed ($Bi = 0$); therefore, this is an isothermal jet and the breakup occurs due to the capillary effects only. The higher pressure at the centre of the jet (neck point) pushes the fluid toward the sides (swell points). The sinusoidal shape of the surface is conserved during most of the breakup time; however, nonlinearities finally take over and the location of the point with the minimum radius starts to move away from the centre. Consequently, at the time of breakup, a long ligament is formed between the main drops. Although the computations are stopped at the breakup point, the long ligament will eventually form a spherical satellite drop. Figure 2(*d*) shows the instability of a jet with the same surface temperature distribution as the ambient, i.e.

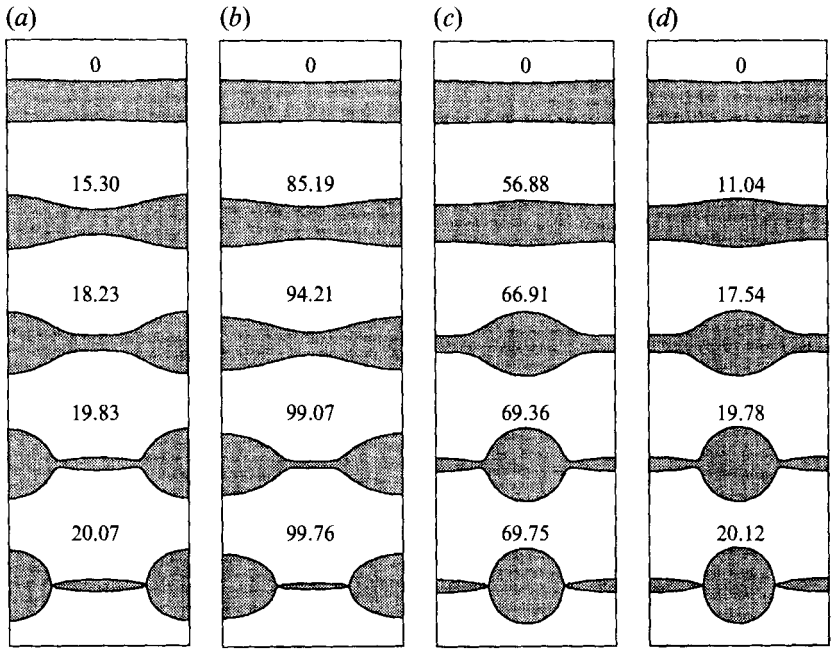

FIGURE 2. Time evolutions of surfaces of four jets with (*a*) $Bi = 0$, (*b*) $Bi = 1.37$, (*c*) $Bi = 1.38$, and (*d*) $Bi = \infty$. For all jets a surface displacement was applied accompanied by a thermal disturbance which increased sinusoidally from 0 at the neck to 1 at the swell of the initial surface disturbance. The initial temperature was $T = 1$; $Re = 20$, $Ma = 200$, $Ca = 0.2$, $k = 0.7$, and $\epsilon_0 = 0.05$ for all jets. The numbers on the figure represent the time. Critical breakup of the jets occurs in the interval $1.37 < Bi < 1.38$.

$T_s(z) = T_a(z)$, as well as a surface disturbance with $\epsilon_0 = 0.05$. This condition represents the limiting case of $Bi = \infty$, where the surface temperature follows that of the ambient due to infinitely large convective heat transfer. Since the surface temperature at the neck is persistently kept lower than that of the swell, the thermocapillary flows overcome the capillary flows and the amplitude of the neck increases. During the remainder of the breakup process thermocapillary and capillary effects are complementary and the disturbance amplitude grows at a faster rate.

The two limiting cases shown in figures 2(*a*) and 2(*d*) indicate that, depending on the relative effects of the capillary and thermocapillary flows, different instability modes can be obtained. Figures 2(*b*) and 2(*c*) show that the transition from the capillary-dominated instability to the thermocapillary-dominated one is not smooth – at the transition point a sudden change in the behaviour of the jet is observed. In this case, the change in the jet behaviour has occurred in the interval of $1.37 < Bi < 1.38$. Determination of the exact critical *Bi* at which the transition occurs is computationally prohibitive. However, the behaviour of the jet in the neighbourhood of the critical *Bi* indicates that the jet is marginally stable at this *Bi* value.

A parameter which implies that the jet is marginally stable at the critical *Bi* is the jet breakup time. The jet breakup time for a large range of *Bi* is shown in figure 3. The breakup time is defined as the time it takes for the radius of the jet to reach a certain minimum value ($r = 0.01$) after which the computation is stopped. When *Bi* is increased from very small values or decreased from very large values the breakup time increases. As *Bi* becomes closer to the critical *Bi* the breakup time increases at a faster rate, such that for $Bi = 1.37$ the breakup time is about five times as large as that of an

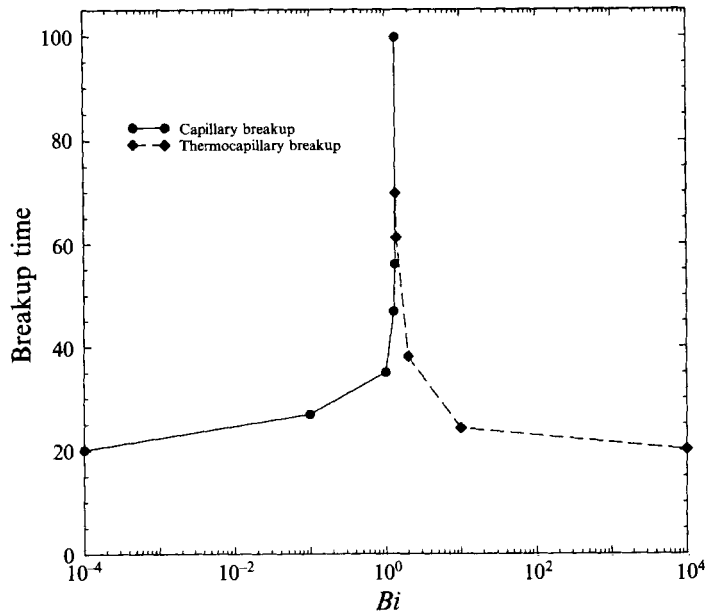

FIGURE 3. Variation of breakup time with Biot number.

Bi	Satellite drop radius	Main drop radius
0	0.575	1.871
0.1	0.474	1.878
1.0	0.398	1.882
1.3	0.366	1.884
1.35	0.355	1.885
1.37	0.329	1.886
1.38	0.620	1.866
1.4	0.614	1.866
2.0	0.615	1.866
10.0	0.656	1.862
∞	0.662	1.861

TABLE 2. Variation of satellite and main drop radius with *Bi*. $Re = 20$, $Ma = 200$, $Ca = 0.2$, $k = 0.7$, and $\epsilon_0 = 0.05$

isothermal jet. These results imply that at the critical *Bi* the breakup time is infinite and the jet is marginally stable. It should be emphasized that this stability point does not mean that the disturbances will damp out, yet the surface of the jet attains a particular configuration such that the capillary and thermocapillary effects continuously cancel each other out.

Variations of the radii of the main (larger) and satellite (smaller) drops produced due to the breakup of the jet with *Bi* are provided in table 2. The radii of the main and satellite drops are calculated based on nominal spherical drops having the same volumes as the two liquid masses produced after the breakup. The radius of the satellite produced with $Bi = 1.38$ is almost twice that of the radius of the satellite produced at $Bi = 1.37$. The satellite radius decreases continuously as *Bi* is increased toward its critical value. Similarly, the satellite radius decreases continuously as *Bi* is decreased

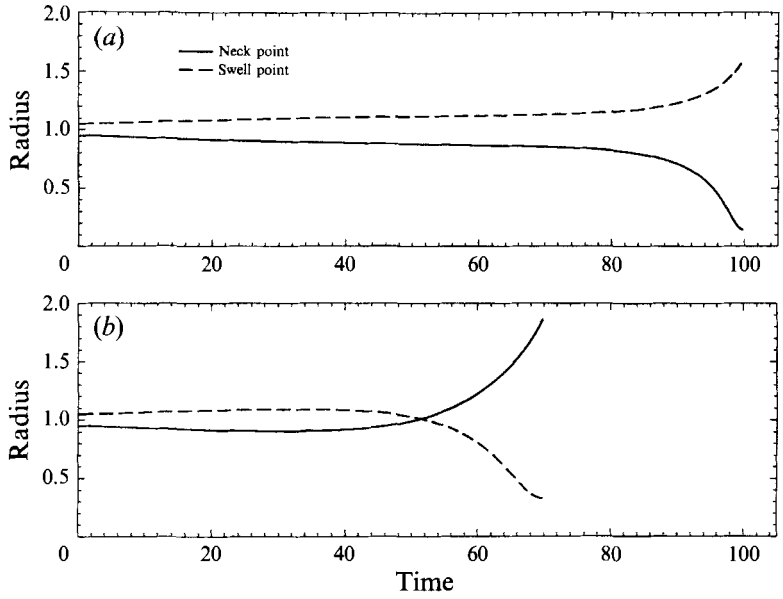

FIGURE 4. Time variations of the radius of the jets at the neck and swell points for (*a*) $Bi = 1.37$ and (*b*) $Bi = 1.38$. Surface evolution and parameter description for these jets are given in figure 2.

toward its critical value. A small increase in the satellite size is noted when Bi is decreased from 1.4 to 1.38. This increase is due to the increase in the breakup time which results in an increase in the surface temperature gradient. For instance, for $Bi = 2.0$, at the time of breakup the surface temperatures at the neck and swell are $T_s(z = 0) = 0.324$ and $T_s(z = \frac{1}{2}\lambda) = 0.997$, respectively, i.e. $\Delta T_s = 0.673$. As Bi is reduced to 1.4, the corresponding temperatures are $T_s(z = 0) = 0.359$ and $T_s(z = \frac{1}{2}\lambda) = 0.994$, i.e. $\Delta T_s = 0.635$. Therefore, a reduction in Bi causes a reduction in the surface temperature gradient and, consequently, a weaker thermocapillary effect. However, as Bi is further reduced to $Bi = 1.38$, the corresponding surface temperatures become $T_s(z = 0) = 0.345$ and $T_s(z = \frac{1}{2}\lambda) = 0.992$, i.e. $\Delta T_s = 0.647$. Since the breakup time is increased significantly close to the critical Bi the surface temperature gradient increases slightly and, therefore, so does the satellite size.

Consider the two cases with Bi closest to the critical point, meaning $Bi = 1.37$ and 1.38. Time variation of the radius of the jet at the neck ($z = 0$) and the swell ($z = \frac{1}{2}\lambda$) points is presented in figure 4. Figure 4(*a*) for $Bi = 1.37$ shows that the amplitude of the disturbance at these points increases with a very small rate for about 80% of the breakup time. Up to this time the capillary and thermocapillary forces are of the same order until, finally, owing to the increase of curvature of the surface at the neck region and decrease of curvature at the swell region the capillary forces dominate. It should be mentioned that the thermocapillary effects are also increasing with time owing to the increase of heat transfer to the ambient that produces larger temperature gradients on the surface. In fact, for the case of $Bi = 1.38$ (figure 4*b*) the rate of increase of thermocapillary effects is slightly larger than the rate of increase of capillary forces. Figure 4(*b*) indicates that at $Bi = 1.38$ the capillary effects are dominant in the beginning; however, thermocapillary forces finally overcome and the rates of change of radii of neck and swell are inverted. Similar behaviour is observed for the variations of radial velocities at the neck and swell points (Mashayek 1994).

The competing effects of the capillary and thermocapillary flows can be directly

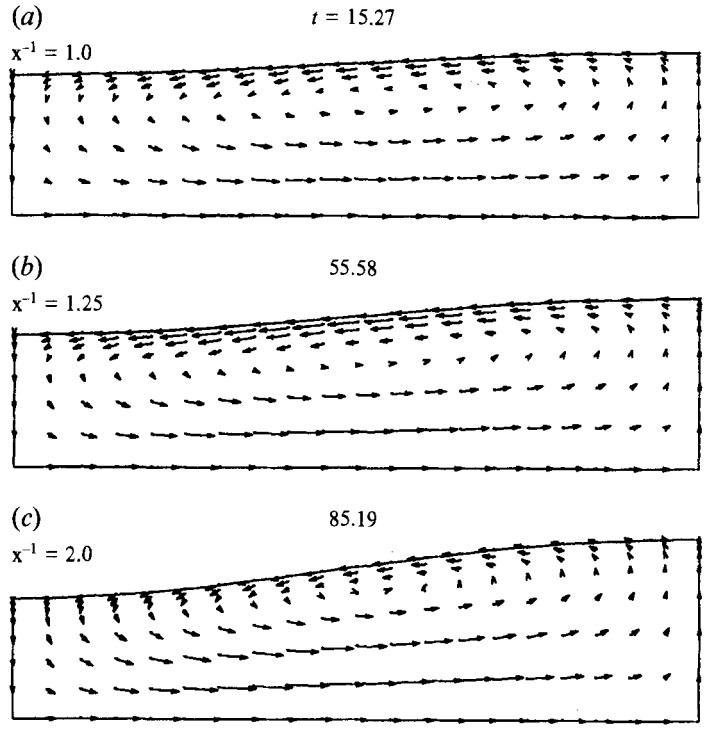

FIGURE 5. Velocity vector plots for the jet with $Bi = 1.37$, shown on figure 2(*b*), at three different times. Numbers above the figures show the time and x represents the scale of the velocity vectors.

observed by studying the velocity fields. Plots of velocity vectors are given in figures 5 and 6 at three different times for $Bi = 1.37$ and 1.38, respectively. Notice that the velocity vectors in each plot are scaled such that the flow fields can be clearly visualized. The scale given on each plot is based on the case with $x = 1$. The first plot of each figure shows the velocity field at an earlier time when the capillary forces are dominant and the net flow is from the neck toward the swell. Because of the transient nature of the problem both capillary and thermocapillary flows increase in time. For $Bi = 1.37$ the capillary forces remain dominant throughout the lifetime of the jet and eventually a substantial net flow is observed from the neck to swell, as shown in figure 5(*c*). A considerable thermocapillary flow is still observed along the surface which retards the growth rate of the surface disturbance. However, for $Bi = 1.38$ the thermocapillary flows eventually dominate and the initial neck and swell points are displaced upward and downward, respectively, as shown in figure 6(*c*). The circulation zone has moved to the left end of the jet close to the axis, and will later move out of the jet entirely. At this time the capillary forces are in the same direction as the thermocapillary forces increasing the growth rate of the disturbance.

In figures 7 and 8 we present the isotherms for the jets with $Bi = 1.37$ and 1.38, respectively. Similarly to the velocity fields, the isotherms for the two cases show small differences during the first half of the breakup time (compare figures 7*a* and 8*a*). However, as soon as the velocity fields start to develop in different directions so do the isotherms. The dominant thermocapillary convective flows deform the isotherms in the direction of the flow field. The largest isotherm deformations are observed in the breakup region owing to the high velocity gradients in this region. Close inspection of isotherms shown in figures 7 and 8, and also isotherm plots shown in other sections of

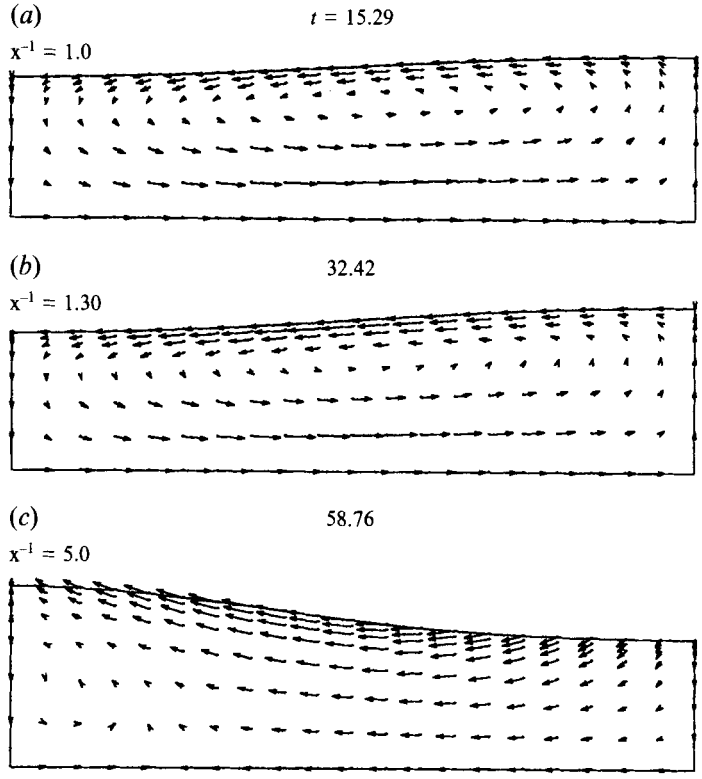

FIGURE 6. As figure 5 but for the jet with $Bi = 1.38$, shown on figure 2(*c*).

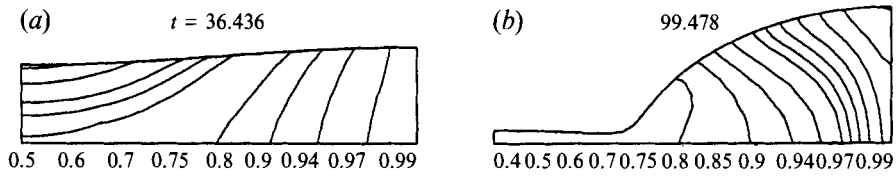

FIGURE 7. Isotherms for the jet of figure 2(*b*) with $Bi = 1.37$ at two different times. Numbers above figures represent the time and numbers below figures show the value of the isotherms. The lowest isotherm on each figure is located close to the top-left corner of that figure.

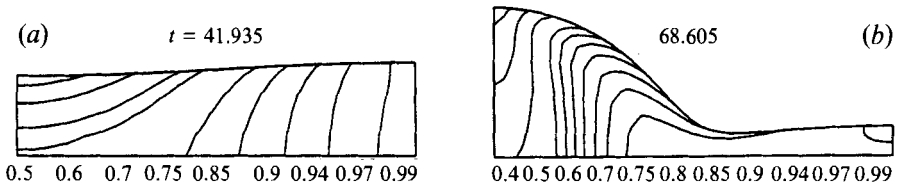

FIGURE 8. As figure 7 but for the jet of figure 2(*c*) with $Bi = 1.38$.

this paper, indicates that in some cases isotherms are not normal to the z-axis which is not consistent with the boundary condition $\partial T/\partial r = 0$ given in (9). The reason is that in these cases $\partial T/\partial z$ is also very close to zero and the isotherms which should be normal to ∇T will not be normal to the z-axis except for very small r. To capture the exact form of isotherms one should use very fine mesh close to the z-axis which would substantially increase computational time. On the other hand, temperature gradients on the z-axis

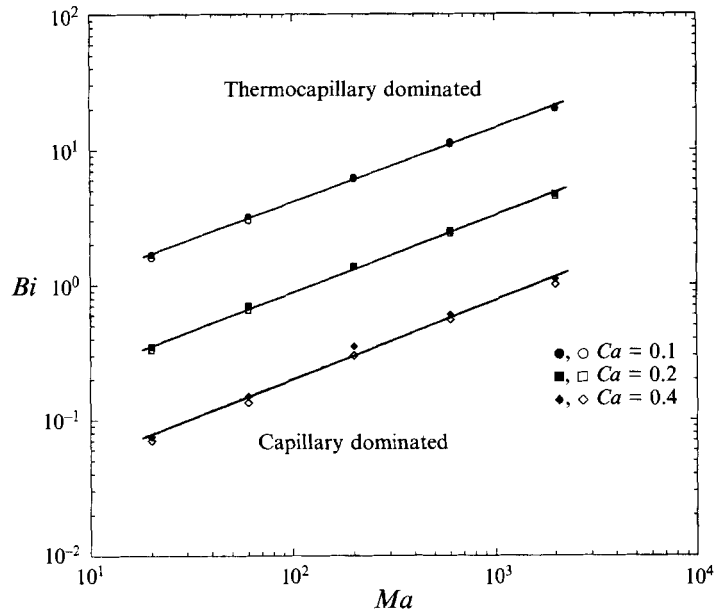

FIGURE 9. Critical surface for jets with $Re = 20$, $k = 0.7$, and $\epsilon_0 = 0.05$. For any pair of Ma and Ca a point is assigned above which the thermocapillary-dominated breakup and below which capillary-dominated breakup occurs.

do not affect the instability of the jet significantly, since thermocapillary flows are induced by temperature gradients along the free surface only. Therefore, in order to have reasonable computational times we have used smaller elements close to the free surface and larger elements near the z-axis. Typical simulations on finer meshes close to the z-axis were also performed and it was verified that changes in the final outcome of the jet instability were negligible. It should be mentioned that similar deviations are also observed in the results provided by other authors (e.g. Cuvelier & Driessen 1986).

Because of its significance, the critical Bi for a wide range of Ma and Ca has been obtained. Other parameters are kept constant at $Re = 20$, $k = 0.7$, and $\epsilon_0 = 0.05$. Figure 9 shows the variation of the critical Bi versus Ma for three different Ca. Two different symbols (filled and non-filled) are shown on the figure to represent the two limiting cases with capillary- and thermocapillary-dominated instabilities. The lower non-filled symbol belongs to the capillary-dominated breakup. Figure 9 shows that decreasing Ca and/or increasing Ma increases the critical Bi. Interestingly, on a log–log plane, the variation of the critical Bi with Ma for any constant Ca is approximately linear. Also, for the range of parameters studied here, the lines for different Ca are approximately parallel. No thermocapillary breakup could be obtained for $Ca < 0.05$ irrespective of the value of Ma. (Re, k, and ϵ_0 were kept constant at 20, 0.7, and 0.05, respectively.) Although the effect of disturbance amplitude, ϵ_0, is not studied here, it is believed that the critical Bi will increase with an increase in ϵ_0, since stronger thermocapillary flows will be required in order to balance the capillary flows.

3.1.2. *Effect of the disturbance wavenumber*

Numerical simulations have been carried out for $Re = 200$, $Ma = 20$, $Ca = 0.02$, $Bi = 10$, $\epsilon_0 = 0.05$, and four different wavenumbers $k = 0.3, 0.5, 0.7, 0.9$. For this study the initial liquid temperature is set at $T = 1$ and the ambient temperature is varied

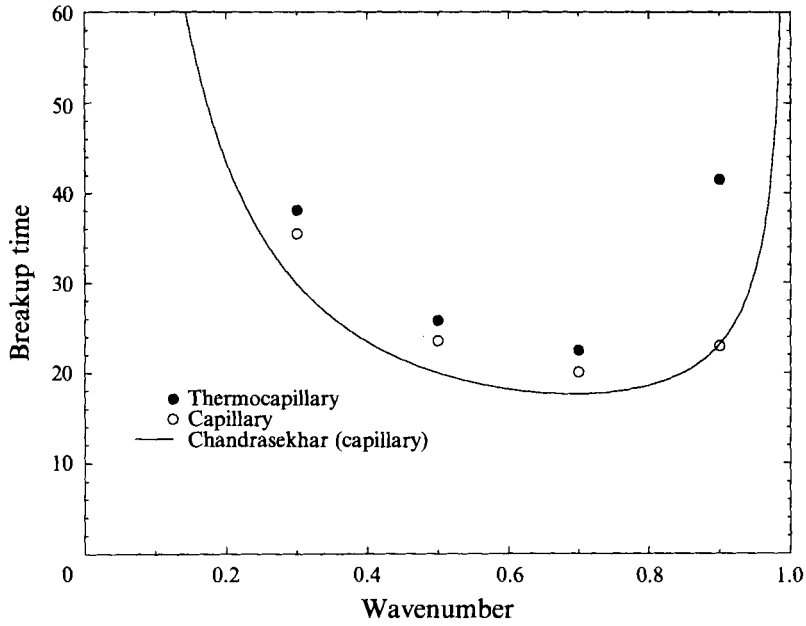

FIGURE 10. Variations of the breakup time versus wavenumber for $Re = 200$, $Ma = 20$, $Ca = 0.02$, $Bi = 10$, and $\epsilon_0 = 0.05$. Solid line represents the results of linear theory by Chandrasekhar (1961) for capillary jets. A surface displacement is considered accompanied by a thermal disturbance which increases sinusoidally from 0 at the neck to 1 at the swell of the initial surface disturbance. The initial temperature is $T = 1$ throughout the jets.

sinusoidally from 0 at the neck, to 1 at the swell. Therefore, the mean temperature of the jet decreases in time. Figure 10 shows the breakup times for cases with and without thermocapillarity along with the analytical curve by Chandrasekhar's (1961) linear theory for viscous capillary jets with $Re = 200$. The analytical curve has been calculated from the growth rate, ω, using the relation: $t_b = \ln(R/\epsilon_0)/\omega$. The results indicate that as the wavenumber increases the thermocapillary jet further deviates from the capillary jet. For a wavenumber of $k = 0.9$ the breakup time of the thermocapillary jet is about twice as large as that of the capillary jet.

Typical curves showing the time variations of logarithmic values of the normalized amplitudes of the swell $((r_s - R)/\epsilon_0)$, the neck $((r_n - R)/\epsilon_0)$ and their difference $((r_s - r_n)/\epsilon_0)$ for two wavenumbers of 0.7 and 0.9 are given in figure 11. Here, r_n and r_s are the radii of the neck and the swell points, respectively. While the curves of the logarithmic amplitudes seem to be linear during most of the breakup process for $k = 0.7$, they obviously are not close to a line for $k = 0.9$. As suggested by Donnelly & Glaberson (1966) the curve of logarithmic difference of the amplitudes of the swell and the neck can be used to calculate an average value for the growth rate (see Mashayek & Ashgriz 1993 for the details). The slope of this curve, when approximated by a straight line, provides the growth rate. The following growth rates could be determined: 0.091, 0.125, and 0.14, for $k = 0.3$, 0.5, and 0.7, respectively. The corresponding growth rates for the isothermal capillary jets are 0.097, 0.135, and 0.16 (Ashgriz & Mashayek 1994). Clearly the opposing directions of the thermocapillary and capillary flows retards the growth rate. In all of the above cases, Bi is less than the critical Bi. Close inspection of figure 11(*b*) reveals that the curves of the amplitudes of the swell and the neck cross each other several times during the first half of the breakup time.

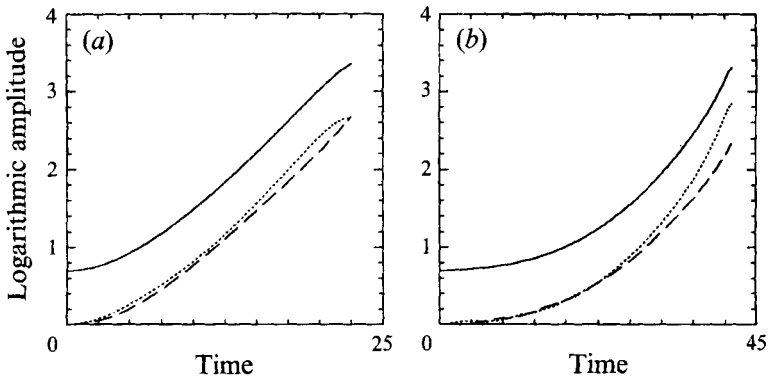

FIGURE 11. Logarithmic variations of the amplitudes of the swell (– – –), neck (. . . . .), and the difference between them (——) versus time for (*a*) $k = 0.7$, and (*b*) $k = 0.9$. Parameters are the same as in figure 10.

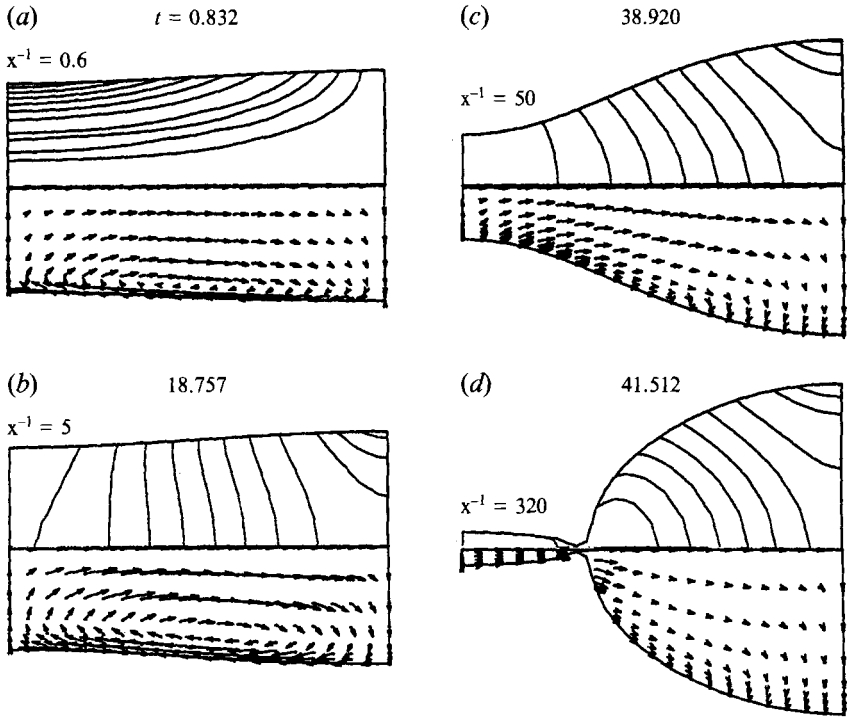

FIGURE 12. Isotherms and velocity vector plots for a jet with $Re = 200$, $Ma = 20$, $Ca = 0.02$, $Bi = 10$, $k = 0.9$, and $\epsilon_0 = 0.05$. The numbers on the figure show the time, and x represents the scale of the velocity vectors.

This indicates the close competition of capillary- and thermocapillary-induced flows during the early stages of the growth of the surface disturbances.

The observed changes of the breakup time with wavenumber can also be explained by considering a typical isotherm and velocity vector plot, as presented in figure 12 for $k = 0.9$. Initially, the interaction of the thermocapillary and capillary forces produces a circulating flow near the free surface. As the radius of the neck reduces, the capillary effects become stronger, dominating the thermocapillary effects, hence suppressing the circulating zone. For $k = 0.9$, the circulating flow survives for a much longer time than

for the smaller wavenumbers. This substantially reduces the growth rate of the surface disturbance and results in a larger breakup time. The effects of the flow on the temperature field are also shown in figure 12. In figure 12(*a*), the isotherms are aligned relatively parallel to the surface, which indicates a small radial conductive heat transfer. The values of the isotherms shown on the figures are 0.1, 0.2, 0.3, 0.4, 0.5, 0.6, 0.7, 0.8, 0.9, 0.94, 0.97 and 0.99. The highest isotherm ($T = 0.99$) in all of the figures is the one closest to the right-top corner. Later in time, in figure 12(*b*), the isotherms become more aligned with the radial direction. At this time the turning of the flow in the swell region entraps the higher isotherms close to the surface. As the pinch-off process occurs and the flow field becomes more non-uniform in the swell region, the isotherms appear to be more distorted. In general, since Pr is small ($Pr = 0.1$) the isotherm pattern is not significantly affected by convective motion.

3.1.3. *Comparison with the linear theory*

The numerical results from this study are compared with the linear solution of XD. They have considered a convective heat transfer with the surroundings which has a linear temperature distribution. In order to analyse the instability of the jet they perturb the basic state for the velocity and temperature fields which has already been calculated for a non-deformable free surface. The case that we have chosen for comparison is identified by $Re = 200$, $Ma = 20$, $Ca = 0.02$, and $Bi = 1$ (which corresponds to their $R_B = 200$, $S = 10^4$, $P = 0.1$, and $B = 1$). The domain of validity of their solution is restricted to small Ca (small deformation for the surface is allowed) and not very small wavenumbers. For the parameter values considered here, XD's equation (6.1) requires $k \gg 0.13$.

To solve the problem we have first developed the basic-state velocity and temperature fields using the same boundary and initial conditions, and the same values for the dimensionless numbers as XD. The simulated basic state is then considered as the initial condition for a jet with the initial surface disturbance amplitude of $\epsilon_0 = 0.01$. There is a difference, however, between our simulated basic state and the one used by XD. They have considered an infinitely long liquid jet rather than a single wavelength of the jet. Therefore, their basic state, contrary to ours, does not have a return flow at the ends of the half-wavelength. The growth rate for the above jet with wavenumber of $k = 0.7$ based on the linear theory of XD is $\omega = 0.15$ – this number is read from their figure 7(*e*) within the accuracy of the thickness of the curve. To calculate the growth rate in our simulation we follow the same procedure as described in §3.1.2. For the case under consideration the calculated growth rate is $\omega = 0.16$ which is very close to the result of XD. It appears that for this particular case the return flow in our simulation has a weak effect on the growth rate. In order to investigate the wavenumber limitation imposed by linear theory ($k \gg 0.13$), we also simulated a case with $k = 0.3$ while other parameters were the same as the previous case. The result of the simulation shows a 34% reduction in growth rate as compared to the prediction of linear theory for $k = 0.3$. Therefore, the wavenumber limitation (XD's equation (6.1)) is rather severe which substantially decreases the range of applicability of the results of linear theory for some range of parameter values of practical interest.

3.2. *Out-of-phase thermal and surface disturbances* ($\theta = 180°$)

In §3.1.1, we studied the evolution of a liquid jet subject to in-phase surface and thermal disturbances and found that for a certain combination of non-dimensional numbers a critical condition existed at which the jet was marginally stable. We also observed that when the thermocapillary-dominated breakup occurred the uni-

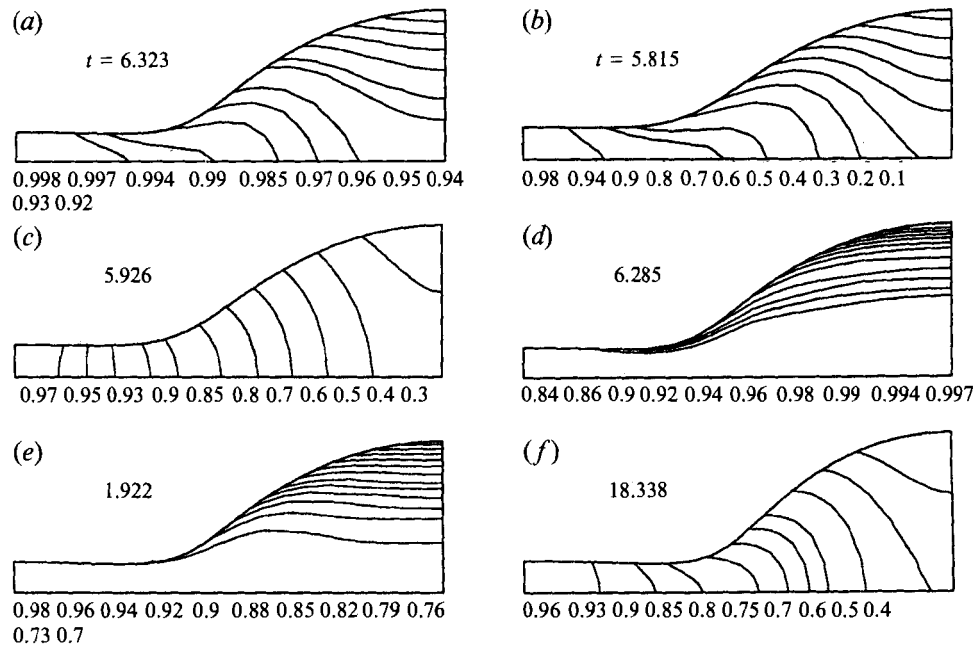

FIGURE 13. Isotherms for jets subject to out-of-phase surface and thermal disturbances. The ambient temperature varied sinusoidally from 1 at the neck to 0 at the swell and the initial temperature was $T = 1$ throughout the jet. Numbers above figures represent the time and numbers below figures show the value of the isotherms. The lowest isotherm on each figure is located close to the top-right corner of that figure. $Re = 20$, $k = 0.7$ and $\epsilon_0 = 0.05$ for all cases. (*a*) $Ma = 20$, $Ca = 0.02$, $Bi = 0.1$; (*b*) $Ma = 20$, $Ca = 0.02$, $Bi = 10$; (*c*) $Ma = 2$, $Bi = 1$; (*d*) $Ma = 200$, $Ca = 0.02$, $Bi = 1$; (*e*) $Ma = 140$, $Ca = 0.002$, $Bi = 0.05$; (*f*) $Ma = 140$, $Ca = 0.2$, $Bi = 0.05$.

directional action of capillary and thermocapillary flows accelerated the breakup. In this section, we consider the effects of out-of-phase surface and thermal disturbances on the jet breakup.

The problem description and the initial conditions remain the same as in §3.1.1, i.e. $T = 1$ and $u = v = 0$ at $t = 0$; however, the thermal boundary condition given in (21) is modified to account for a phase shift of $\theta = 180°$:

$$T_a(z) = 0.5[1 + \cos(kz)]. \tag{22}$$

In this case the neck point is at a higher temperature than the swell point. Therefore, the thermocapillary flows are in the same direction as the capillary flows. In the following simulations, $Re = 20$, $k = 0.7$, $\epsilon_0 = 0.05$ are kept constant and Bi, Ma, and Ca are varied. For each of these non-dimensional numbers we consider two orders of magnitude variations: $Bi = 0.1$, 0.3, 1.0, 3.0 and 10.0, $Ma = 2.0$, 6.0, 20.0, 60.0 and 200.0, and $Ca = 0.002$, 0.006, 0.02, 0.06, 0.12 and 0.2. We begin our discussion by considering the isotherm plots for the two limiting cases of each parameter. The times at which the shapes of the jets are similar are considered. Figure 13(*a*, *b*) shows isotherms for $Bi = 0.1$ and 10 while $Ma = 20$ and $Ca = 0.02$ are kept constant. The values of the contours are different in the two figures and are given below each figure. Comparison of the two figures reveals that increasing Bi does not affect the shape of the isotherms and simply results in a cooler jet. Increasing Bi enhances the temperature gradient along the surface and strengthens the thermocapillary-induced flows. However, for the range of parameters considered here, it did not alter the overall flow field substantially. When Ma was changed by two orders of magnitude from 2 to 200

Bi	*Ma*	*Ca*	$\frac{t_{th}-t_{ca}}{t_{ca}}\times 100$	$\frac{R_{th}-R_{ca}}{R_{ca}}\times 100$
0.1	20	0.02	0.79	0.29
0.3	20	0.02	0.26	0.77
1	20	0.02	−1.11	1.99
3	20	0.02	−3.18	3.38
10	20	0.02	−5.31	4.13
1	2	0.02	−3.96	3.53
1	6	0.02	−2.45	2.96
1	60	0.02	−0.28	1.28
1	200	0.02	0.3	0.71
1	20	0.002	−0.02	0.14
1	20	0.006	−0.19	0.53
1	20	0.06	−4.31	6.64
1	20	0.12	−9.07	13.56
1	20	0.2	−14.19	21.78

TABLE 3. Percent relative change in breakup time and satellite radius. $Re = 20$, $k = 0.7$, and $\epsilon_0 = 0.05$

($Bi = 1.0$ and $Ca = 0.02$) the isotherms changed significantly as seen in figure 13(*c*, *d*). This can be explained by considering that the increase of *Ma*, while *Re* is constant, corresponds to decrease of thermal conductivity, κ. In figure 13(*c*) the conductive heat transfer is dominant and the isotherms are aligned radially because the heat transferred to the jet at the surface is conducted to the core fluid quickly. However, the weak conduction effects at high *Ma* results in the alignment of the isotherms with the flow direction as seen in figure 13(*d*).

Increase of *Ca* affects the isotherms inversely as compared to *Ma*. An increase in *Ca*, keeping *Ma* constant, indicates a decrease in the surface tension of the liquid, α_0'. Therefore, the capillary forces become smaller and the surface disturbances grow slower. Figures 13(*e*) and 13(*f*) show that increasing *Ca* from 0.002 to 0.2, keeping *Bi* and *Ma* constant at 1.0 and 20, respectively, results in more radially aligned isotherms. This variation of the shapes of the isotherms with *Ca* can be explained by comparing the magnitude of the velocities and the times corresponding to the similar shapes of the two jets. For instance, the magnitudes of the velocities obtained for the jet with $Ca = 0.002$ are about one order of magnitude larger than for the jet with $Ca = 0.2$. This means that the convective heat transfer must be an order of magnitude stronger for the case with $Ca = 0.002$. On the other hand, the elapsed time is about one order of magnitude smaller for the smaller *Ca* of 0.002, indicating less time for conductive heat transfer for smaller *Ca*. Therefore, for the jet with $Ca = 0.002$ the relative strength of convective to conductive heat transfer is about two orders of magnitude larger than the jet with $Ca = 0.2$ and the isotherms are aligned with the flow field.

The influence of the various non-dimensional numbers on the breakup time and satellite drop radius are determined and compared with those of pure capillary breakup. In table 3 the percentage change in the breakup time and satellite radius are given versus *Bi* ($Ma = 20$ and $Ca = 0.02$), *Ma* ($Bi = 1.0$ and $Ca = 0.02$) and *Ca* ($Bi = 1.0$ and $Ma = 20$). Percentage change of breakup time is defined as the difference between the breakup time of the thermocapillary (t_{th}) and the isothermal capillary (t_{ca}) jets divided by the breakup time of the capillary jet, i.e. $[(t_{th}-t_{ca})/t_{ca}]\times 100$. Similarly

the percentage change of drop radius is defined as the difference between the drop radii obtained by the thermocapillary instability (R_{th}) and capillary instability of the isothermal jet (R_{ca}) divided by the latter, i.e. $[(R_{th}-R_{ca})/R_{ca}]\times 100$. The breakup time decreases with increasing Bi and/or decreasing Ma as seen in table 3. Breakup time also decreases with increasing Ca. In general, for all the cases studied here, thermocapillarity decreases the breakup time within 15% of the pure capillary breakup time. (Small increases in breakup time are observed for small Bi or large Ma). The variations of the satellite radius with the non-dimensional parameters is opposite to the variations of the breakup time. Table 3 shows that thermocapillarity increases the satellite size for all the cases up to 22% larger than the size of the satellite produced due to the capillary breakup only. Therefore, out-of-phase surface and thermal disturbances are not very effective in reducing the satellite size.

4. Spatially uniform ambient temperature

4.1. *Thermal disturbance with no surface disturbance*

In this section we consider the temporal instability of a cylindrical liquid jet exposed to a spatially uniform ambient temperature and subject only to an initial thermal disturbance at its surface and no surface displacement. In order to obtain approximate values of the non-dimensional numbers involved in practice, consider a water jet with radius of 100 μm issuing into ambient air at a slightly different temperature. The temperature of the water in the supply tank and the ambient air are assumed to be at $T'_0 = 20$ °C and $T'_a = 25$ °C, respectively. Using the properties of water and air at these temperatures, we obtain $Ca = 0.01$, $Re = 20$, and $Ma = 140$. Assuming pure natural convection between the jet and ambient air, $Bi = 0.012$ is obtained for a 5 °C temperature difference. However, since in most practical situations the jet velocity relative to air is large, we expect that Bi to be at least one order of magnitude larger.

The effect of a wide range of parameters on the thermocapillary instability of a liquid jet issuing from a nozzle into a spatially uniform ambient is investigated. In an attempt to characterize the breakup of the jet we have considered a periodic thermal disturbance imposed on the jet surface at the nozzle exit as

$$T_s(z) = 0.5[1+\cos(kz)] \quad \text{at} \quad t=0 \quad \text{and} \quad r=1. \tag{23}$$

It is assumed that T'_0 is the initial temperature of the liquid in the supply tank and $\Delta T' = T'_a - T'_0$. Therefore, the dimensionless ambient temperature is constant at $T_a = 1$ and the initial jet temperature is $T(z, r) = 0$ except on the surface which is given by (23). Notice that (23) expresses an initial condition to the problem rather than a boundary condition as discussed in §3. Boundary conditions are given by (6) and (8)–(10).

A two orders of magnitude variation in Bi, Ma, and Ca was considered. Reynolds number and wavenumber were kept constant at $Re = 20$ and $k = 0.7$. Numerical simulations were performed for three different values of Biot number ($Bi = 0.05$, 0.5 and 5.0), Marangoni number ($Ma = 14$, 140 and 1400), and capillary number ($Ca = 0.001$, 0.01, and 0.1). A 40×9 element mesh was implemented for the simulations with compressed elements near the free surface to resolve both the hydrodynamic and thermal boundary layers. The axial direction was discretized uniformly by 40 elements. Results show that a periodic thermal disturbance induces a surface displacement with the same wavenumber, but with a 180° phase shift.

Generally, the results indicate that the isotherms are aligned with the free surface and follow the evolution of the surface during the earlier times. This is due to the relatively large Pr, ranging from 0.7 to 70. A typical case for $Ma = 140$, $Ca = 0.01$ and $Bi = 0.5$

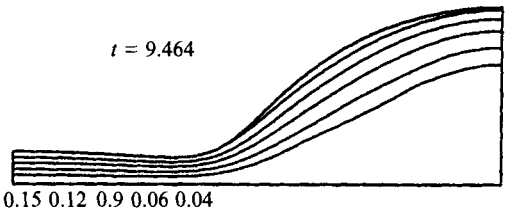

FIGURE 14. Typical shape and isotherms of a jet subject to initial thermal disturbance varied sinusoidally from 1 at the neck to 0 at the swell on the surface, shortly before the breakup. Initial temperature was $T = 0$ throughout the jet and the ambient temperature was constant at $T = 1$. The number above the figure shows the time and numbers below the figure represent the value of the isotherms. The highest isotherm on each figure is located close to the top-left corner of that figure. $Re = 20$, $Ma = 140$, $Ca = 0.01$, $Bi = 0.5$, and $k = 0.7$.

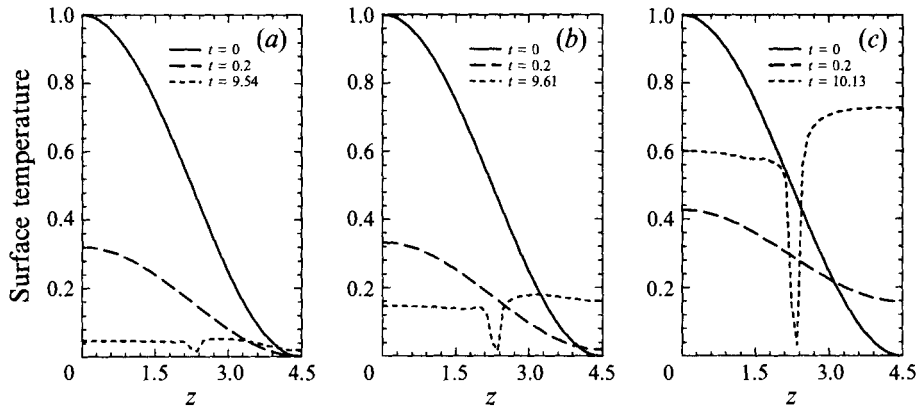

FIGURE 15. Variations of the surface temperature for jets with $Ma = 140$, $Ca = 0.01$, and (*a*) $Bi = 0.05$, (*b*) $Bi = 0.5$, and (*c*) $Bi = 5$. The solid line represents the initial surface temperature disturbance. The curve with highest time belongs to the surface temperature distribution at the time of breakup.

is shown in figure 14. During the early stages of heat transfer, the isotherms are closely concentrated around the free surface; however, the spacing between the isotherms increases with time. An increase of Bi corresponds to an increase of convective heat transfer from the ambient which results in a warmer jet. An increase of Ma enhances the interaction between the hydrodynamics and heat transfer. As mentioned by other authors (Cuvelier & Driessen 1986; Shen *et al.* 1990), high Ma results in distorted isotherms. This can be explained by realizing that an increase in Ma, while Re is constant, corresponds to an increase in Pr or a decrease of thermal conductivity, κ. Therefore, the upward convective heat transfer overcomes the downward conduction of heat and the ends of the isotherms are turned toward the free surface. For a constant Re, a decrease in Ca can be interpreted as an increase in the coefficient of of surface tension, α_0'. Therefore, as discussed earlier the breakup time is decreased by decreasing Ca, and a shorter time is available for the conduction of heat inside the bulk of the liquid.

In order to investigate whether the surface temperature retains its initial sinusoidal profile, we have plotted the time evolution of the temperature distribution along the surface in figure 15 for three different Bi of 0.05, 0.5, 5.0, with $Ma = 140$ and $Ca = 0.01$. The solid curve in each figure represents the initially imposed surface temperature as given by (23). The distribution shown by the dashed line corresponds to time

Bi	*Ma*	*Ca*	Breakup time	Satellite radius
0.05	140	0.01	9.544	0.558
0.5	140	0.01	9.609	0.558
5	140	0.01	10.129	0.558
0.05	14	0.01	10.867	0.558
0.05	1400	0.01	8.274	0.561
0.05	140	0.001	3.666	0.575
0.05	140	0.1	24.884	0.519

TABLE 4. Variation of breakup time and satellite radius. $Re = 20$, and $k = 0.7$

$t = 0.02$ and indicates that the amplitude of the initially imposed thermal disturbance drops substantially in a short time. However, the sinusoidal profile is conserved up to this stage. The next curve on each figure, shown by the dotted line, depicts the surface temperature distribution at the time of the breakup. No sinusoidal distribution is observed at this time. The sharp decrease of the surface temperature at the breakup point is attributed to the sudden decrease of the surface radius at this point and the flow of a colder core fluid through the pinch-off area. Generally, distributions shown in figure 15 indicate that higher surface temperatures are obtained with higher *Bi*. They also indicate that the surface temperature profiles resemble the jet surface at different times. The largest deviation occurs at the swell point where the temperature profile is at its lowest level and surface shape has its highest radius. The correspondence of surface temperature profile to free surface shape is enhanced when *Bi* is increased.

Variations of breakup time with *Bi*, *Ma* and *Ca* are provided in table 4. Although *Bi* is varied by two orders of magnitude, the breakup times does not change substantially. However, slightly larger breakup times are obtained at higher *Bi*. For these cases, $M = 140$ and $Ca = 0.01$ were kept constant. Table 4 also shows the variation of the breakup time with *Ma*, for $Bi = 0.05$ and $Ca = 0.01$. Interestingly, within this range of *Ma* the breakup times varies linearly with the logarithm of *Ma*. Roughly, a 15% change in breakup time is observed when *Ma* is changed by one order of magnitude. The largest variation of breakup time is obtained by changing *Ca* (for constant $Bi = 0.05$ and $Ma = 140$) as seen in the table. For a constant *Re*, equation (1) shows that a small *Ca* corresponds to a large surface tension coefficient. Therefore, decreasing *Ca* increases the capillary effects and makes the jet breakup faster.

Similar results are obtained for the variations of the satellite drop size with *Bi*, *Ma*, and *Ca* as given in table 4. Within the range of *Bi* studied here ($0.05 < Bi < 5.0$), no considerable change in the satellite size is observed. However, a small increase in satellite radius is obtained by changing *Ma* by two orders of magnitude. Table 4 shows that the largest variation of satellite size is achieved when *Ca* is changed in the interval of $0.001 < Ca < 0.1$. Generally, an inverse proportionality for the breakup time and the satellite size is observed. Smaller capillary forces result in smaller growth rates; consequently, the breakup times increase. On the other hand, smaller capillary forces result in the reduction of the convective fields; consequently, the flow nonlinearities decrease, resulting in a decrease in the satellite size.

4.2. *Thermal disturbance with surface disturbance*

Thus far we have studied the behaviour of a capillary jet subject only to thermal disturbances. However, there are many practical situations in which a thermal disturbance is accompanied by a surface disturbance. In order to evaluate the relative

	Breakup time		Satellite radius	
	$\epsilon_0 = 0.0001$	$\epsilon_0 = 0.5$	$\epsilon_0 = 0.0001$	$\epsilon_0 = 0.05$
Capillary	13.088	4.600	0.5581	0.556
Thermocapillary	9.958	4.592	0.5584	0.556

TABLE 5. Relative effects of the thermal disturbance on the breakup time and satellite radius of a jet

importance of these disturbances, we impose a surface disturbance on the jet as given by (20), in addition to the thermal disturbance given by (23). Obviously, the initial disturbance amplitude, ϵ_0, is an important parameter in this problem and it is expected that for large ϵ_0 capillary effects dominate the thermocapillary effects. Therefore, it is reasonable to perform some simulations to find the range of values for ϵ_0 which allows a close competition between the two effects. In table 5 we present a quantitative comparison of the breakup time and satellite radius for two different cases with $\epsilon_0 = 0.0001$ and 0.05. The corresponding results for a similar jet without thermocapillary effects are also given in this table to provide a direct assessment of the relative importance of thermal disturbances. Other parameters for this problem are $Re = 20$, $Ca = 0.01$, $Ma = 140$, $Bi = 5$, and $k = 0.7$. Comparison of the results obtained with and without thermal disturbance for the jet with the initial surface disturbance amplitude of $\epsilon_0 = 0.05$ indicates the absolute dominance of the capillary effects. The relative changes in the breakup time and satellite size are negligible when the thermal disturbance is superimposed on the surface disturbance. However, results for the case with $\epsilon_0 = 0.0001$ are promising and a relative change of 24% in breakup time is obtained by adding the thermal disturbance. The satellite size, however, remains relatively unchanged for this initial amplitude. Therefore, it is concluded that for the range of parameters considered here (i.e. a 5 °C difference between the water jet and the ambient temperatures), the amplitude of the initial disturbance must be very small for the thermal disturbances to be effective in the breakup of the jet.

5. Discussion and conclusions

The temporal instability of a capillary jet with constant properties reduces to the study of mainly three parameters, namely the Reynolds number based on the liquid properties, $Re_p = (1/\nu)(\alpha_0' R_0'/\rho)^{1/2}$, the initial disturbance wavenumber, k, and its amplitude, ϵ_0. When the properties are allowed to change, the problem becomes much more complex, since not only are more parameters introduced but also the behaviour of the liquid jet may substantially change in time. Therefore, the linear theories, which are only valid at small times, cannot correctly predict the instability conditions of such systems.

Here, we have considered the temperature dependency of the liquid surface tension, and investigated the so-called thermocapillary instability of a liquid jet. The problem is governed by the parameters given in (1), namely Re, Ca, $Ma = Re\,Pr$, and Bi. Since for most practical situations $Re \sim O(10)$, and it has already been shown that for $Re > 10$ there is no significant change in the behaviour of the liquid jet, this parameter is kept constant in our investigation. Therefore, only the effect of Ca, Bi, and Ma are considered. Keeping Re constant means that the variation of Ma represents the effect of Pr or the thermal conductivity of the liquid, κ. The amplitudes of the thermal and

Ca	a	b
0.1	0.54918	−1.11955
0.2	0.56436	−2.72452
0.4	0.58545	−4.32978

TABLE 6. Constants a and b used in equation (24) for different Ca

surface disturbances are mainly kept constant, and their detailed effect on the jet instability is not investigated here. Limitation of the problem to the above parameters was necessary to make it computationally manageable.

The thermocapillary instability of an axisymmetric liquid jet is investigated subject to two different conditions. In the first case a cylindrical liquid jet (an infinitely long liquid column) was suddenly exposed to an ambient with a spatially periodic temperature distribution along the axis of the jet. In the second case an initial thermal disturbance was imposed only on the surface of the liquid while the ambient temperature was kept spatially and temporally uniform.

In the first case, the jet was also given an initial surface disturbance with the same wavenumber as the thermal disturbance of the ambient. Again, two conditions are considered: in-phase and out-of-phase thermal and surface disturbances. When thermal and surface disturbances are in-phase, thermocapillary- and capillary-induced flows are in the opposite direction to each other. For a constant Re, Bi controls the thermal convection to the ambient, and Ma controls the thermal diffusion from the surface to the liquid interior. Together, they control the transient variation of the temperature along the liquid surface and, therefore, the extent of the thermocapillary flows. On the other hand, for a constant Re, Ca is an indicator of the capillary flows in the absence of the thermocapillarity. The results of §3.1 indicate that if the disturbances can be made such that the capillary and thermocapillary flows are in opposite directions, a parameter range can be obtained where they cancel each other. Consequently, a marginally stable jet can be obtained for all the wavenumbers. Figure 9 defines a critical surface in the (Bi, Ma, Ca)-space at which the jet is marginally stable. The critical curves for $k = 0.7$ and $Ca = 0.1$, 0.2 and 0.4 can be represented by

$$Bi = Ma^a + \exp(b), \tag{24}$$

where a and b are functions of Ca and are given in table 6. The following fit to the critical surface can be obtained:

$$Bi = 1.578 \times 10^{-3} Ca^{-2.3157} Ma^{(0.1187Ca+0.5386)}. \tag{25}$$

For $Ca < 0.05$ and for the parameter range studied here, no critical point was observed and the jet instability was always governed by capillary effects. An increase in the disturbance wavenumber (decrease in the wavelength), keeping the thermal disturbance constant, results in an increase in the thermocapillary effects and, therefore, the jet becomes stable at even lower Bi (see §3.1.2). The effect of the disturbance wavenumber and its amplitude on the critical surface are not quantified here.

Information on the conditions that render a jet stable can be useful in designing a controlled environment for the attainment of long liquid columns. Such columns are useful in containerless processing of single crystals. For a stationary liquid column, design of an environment with periodic temperature variation is practicable. However, the application of such a thermal boundary condition to control the breakup of a moving jet is a more complicated task. For a liquid jet, the temperature of the ambient

has to be controlled such that each point on the surface of the jet is continuously exposed to a constant local ambient temperature. This condition can be attained by making the ambient temperature periodic in both space and time.

If the thermocapillary flows are in the same direction as the capillary flows, the originally unstable jet cannot be stabilized. Such thermal effects can, however, be used to somewhat control the breakup time and the satellite size. The results indicate that an increase in *Bi* or a decrease in *Ma* decreases the breakup time as compared to the isothermal jet. The breakup times generally decrease on increasing *Ca*. The satellite sizes generally increase because of the thermocapillary effects. The satellite size is mainly determined based on the mean convective velocities, which are generally larger because of the complementing thermocapillary flows.

In addition, the thermocapillary instability of a liquid jet exposed to a spatially uniform ambient temperature is also investigated. Here, an initial thermal disturbance is imposed only on the liquid surface. Two cases are considered. In the first case, an initial temperature disturbance is imposed on the surface of the liquid without any surface disturbance. This problem has important natural and physical implication. The natural instability and breakup of a liquid jet issuing from a nozzle is an everyday experience. Since the time of Rayleigh (1879) this instability was considered to be due to surface, pressure, or velocity disturbances. The results in §4.1 clearly show that a small temperature disturbance can quickly induce a surface disturbance which will eventually cause the breakup of the jet. Such temperature disturbances are readily available in most natural processes, since upon exiting from the nozzle the liquid temperature is usually slightly different than the ambient temperature. For the small thermal disturbance amplitudes studied here, the results indicate that neither the breakup time nor the satellite size are sensitive to *Bi* and *Ma*; however, they are sensitive to *Ca*. In other words, the initial thermal disturbance only induces a small surface disturbance which basically governs the instability of the jet thereafter.

In §4.2 it is shown that if, in addition to the initial thermal disturbance, a surface disturbance is also imposed on the jet, the latter will dominate if the initial amplitude ratio of the surface to thermal disturbance is relatively large. For the parameter range studied here, surface disturbance amplitude had to be smaller than $\epsilon_0 = 0.0001$ to see a significant change in breakup times and satellite sizes. This explains the experimental results of Faidley & Panton (1990) who did not see a significant effect on the breakup of the jet when applying a thermal disturbance on the jet at the nozzle. Their initial thermal disturbance was not large enough to significantly alter the original capillary instability conditions. More promising results were obtained in the experiments of Nahas & Panton (1991) when a larger thermal disturbance was imposed on the jet using radiation from a laser source. In general, strong initial thermal disturbances, with the condition that the induced thermocapillary flows be in the opposite direction to the capillary flows, are needed to control the jet instability and obtain stable jets.

REFERENCES

ASHGRIZ, N. & MASHAYEK, F. 1994 Temporal analysis of capillary jet breakup. *J. Fluid Mech.* (submitted).

BAUER, H. F. 1984 Free liquid surface response induced by fluctuations of thermal Marangoni convection. *AIAA J.* **22**, 421–428.

CHANDRASEKHAR, S. 1961 *Hydrodynamic and Hydromagnetic Stability*. Clarendon.

CHAUDHARY, K. C. & REDEKOPP, L. G. 1980 The non-linear capillary instability of a liquid jet. Part 1. Theory. *J. Fluid Mech.* **96**, 257–274.

COWLEY, S. J. & DAVIS, S. H. 1983 Viscous thermocapillary convection at high Marangoni number. *J. Fluid Mech.* **135**, 175–188.

CUVELIER, C. & DRIESSEN, J. M. 1986 Thermocapillary free boundaries in crystal growth. *J. Fluid Mech.* **169**, 1–26.

DAVIS, S. H. 1987 Thermocapillary instabilities. *Ann. Rev. Fluid Mech.* **19**, 403–435.

DIJKSTRA, H. A. & STEEN, P. H. 1991 Thermocapillary stabilization of the capillary breakup of an annular film of liquid. *J. Fluid Mech.* **229**, 205–228.

DOI, T. & KOSTER, J. N. 1993 Thermocapillary convection in two immiscible liquid layers with free surface. *Phys. Fluids* A **5**, 1914–1927.

DONNELLY, R. J. & GLABERSON, W. 1966 Experiment on capillary instability of a liquid jet. *Proc. R. Soc. Lond.* A **290**, 547–556.

FAIDLEY, R. W. & PANTON, R. L. 1990 Measurement of liquid jet instability induced by surface tension variations. *Expl Thermal Fluid Sci.* **3**, 383–387.

FROMM, J. E. 1984 Numerical calculation of the fluid dynamics of drop-on-demand. *IBM J. Res. Dev.* **28**, 322–333.

FU, B.-I. & OSTRACH, S. 1985 Numerical solutions of thermocapillary flows on floating zones. In *Transport Phenomena in Material Processing, Power Eng. Div.* vol. 29, p. 1. ASME.

GOEDDE, E. F. & YUEN, M. C. 1970 Experiments on liquid jet instability. *J. Fluid Mech.* **40**, 495–511.

HADID, H. B. & ROUX, B. 1990 Thermocapillary convection in long horizontal layers of low-Prandtl-number melts subject to a horizontal temperature gradient. *J. Fluid Mech.* **221**, 77–103.

HUGHES, T. J. R., LIU, W. K. & BROOKS, A. 1979 Finite element analysis of incompressible viscous flows by penalty function formulation. *J. Comput. Phys.* **30**, 1–60.

KAZARINOFF, N. D. & WILKOWSKI, J. S. 1990 Bifurcations of numerically simulated thermocapillary flows in axially symmetric float zones. *Phys. Fluids* A **2**, 1797–1807.

KUHLMANN, H. 1989 Small amplitude thermocapillary flow and surface deformations in a liquid bridge. *Phys. Fluids* A **1**, 672–677.

KUHLMANN, H. C. & RATH, H. J. 1993 Hydrodynamic instabilities in cylindrical thermocapillary liquid bridges. *J. Fluid Mech.* **247**, 247–274.

MANSOUR, N. N. & LUNDGREN, T. S. 1990 Satellite formation in capillary jet breakup. *Phys. Fluids* A **2**, 1141–1144.

MASHAYEK, F. 1994 Numerical study of capillary and thermocapillary jets and drops. PhD thesis, State University of New York at Buffalo.

MASHAYEK, F. & ASHGRIZ, N. 1993 A height-flux method for simulating free surface flows and interfaces. *Intl J. Numer. Meth. Fluids* **17**, 1035–1054.

NAHAS, N. M. & PANTON, R. L. 1991 Control of surface tension flows – Instability of a liquid jet. *Trans. ASME* I: *J. Fluids Engng* **112**, 296–301.

OSTRACH, S. 1982 Low-gravity fluid flows. *Ann. Rev. Fluid Mech.* **14**, 313–345.

PLATEAU, J. 1873 Statique experimental et theorique des liquids soumis aux seules forces moleculaires. (Cited by Lord Rayleigh, *Theory of Sound*, vol. II, p. 363, 1945. Dover.)

RAYLEIGH, LORD 1879 On the instability of jets. *Proc. Lond. Math. Soc.* **10**, 4–13.

RUSSO, M. J. & STEEN, P. H. 1989 Shear stabilization of the capillary breakup of a cylindrical interface. *Phys. Fluids* A **1**, 1926–1937.

SEN, A. K. & DAVIS, S. H. 1982 Steady thermocapillary flows in two-dimensional slots. *J. Fluid Mech.* **121**, 163–186.

SHEN, Y., NEITZEL, G. P., JANKOWSKI, D. F. & MITTELMANN, H. D. 1990 Energy stability of thermocapillary convection in a model of the float-zone crystal-growth process. *J. Fluid Mech.* **217**, 639–660.

SHOKOOHI, F. & ELROD, H. G. 1987 Numerical investigation of the disintegration of liquid jets. *J. Comput. Phys.* **71**, 324–342.

SMITH, M. K. 1986 Instability mechanisms in dynamic thermocapillary liquid layers. *Phys. Fluids* **29**, 3182–3186.

SMITH, M. K. & DAVIS, S. H. 1982 The instability of sheared liquid layers. *J. Fluid Mech.* **121**, 187–206.

SMITH, M. K. & DAVIS, S. H. 1983*a* Instabilities of dynamic thermocapillary liquid layers. Part 1. Convective instabilities. *J. Fluid Mech.* **132**, 119–144.

SMITH, M. K. & DAVIS, S. H. 1983*b* Instabilities of dynamic thermocapillary liquid layers. Part 2. Surface-wave instabilities. *J. Fluid Mech.* **132**, 145–162.

VASSALLO, P. & ASHGRIZ, N. 1991 Satellite formation and merging in liquid jet breakup. *Proc. R. Soc. Lond.* A **433**, 269–286.

XU, J. J. & DAVIS, S. H. 1983 Liquid bridges with thermocapillarity. *Phys. Fluids* **26**, 2880–2886.

XU, J. J. & DAVIS, S. H. 1984 Convective thermocapillary instabilities in liquid bridges. *Phys. Fluids* **27**, 1102–1107.

XU, J. J. & DAVIS, S. H. 1985 Instability of capillary jets with thermocapillarity. *J. Fluid Mech.* **161**, 1–26 (referred to herein as XD).

YUEN, M. C. 1968 Non-linear capillary instability of a liquid jet. *J. Fluid Mech.* **33**, 151–163.